
Understanding the Mechanism of Glass Removal in Magnetorheological Finishing (MRF)

Introduction

Two magnetorheological (MR) fluids are currently in widespread industrial use for the commercial manufacture of high-precision optics using magnetorheological finishing (MRF). One composition, which consists of cerium oxide in an aqueous suspension of magnetic carbonyl iron (CI) powder, has been found appropriate for almost all soft and hard optical glasses and low-expansion glass-ceramics. The second composition, which uses nanodiamond powder as the polishing abrasive, is better suited to calcium fluoride, IR glasses, hard single crystals (i.e., silicon and sapphire), and very hard polycrystalline ceramics (i.e., silicon carbide).

The extension of MRF to a vast array of materials is possible because of the unique nature of this finishing process. The magnetic carbonyl iron particles may be thought of as a form of variable compliance lap that supports the nonmagnetic polishing abrasives. Lap stiffness may be increased or decreased by adjusting the CI concentration and/or the magnetic field strength.

Considerations leading to a choice of nonmagnetic polishing abrasive are more complex than those encountered in conventional pitch or pad polishing. Not only do the hardness and chemistry of the abrasive grains need to be appropriate to the workpiece, but the type of abrasive (median size, surface chemistry) can have a large or small effect on the out-of-field MR fluid rheology. Fluid properties in an MRF machine circulation system must be held constant to realize constant rates of material removal during polishing.

Advances have been made in understanding the mechanism of removal with MRF, based in part on the hardness of the CI powder, the magnetorheological properties of the MR fluid, and the interaction of cerium oxide or other abrasives with the workpiece surface. This article presents the results of recent studies, within the context of classical optical polishing operations.

The mechanisms of material removal important to glass polishing have been an area of study for years. Cumbo¹ describes the goals of precision polishing to be to shape the glass to within $0.1 \mu\text{m}$ of the desired form, to remove subsurface damage created by grinding operations, and to reduce the peak-to-valley (p-v) roughness to less than 5 nm. While there are several proposed mechanisms of material removal in polishing, none are widely accepted. Some authors describe polishing in terms of small-scale fracture,^{2,3} while others describe it as “plastic scratching” of a hydrated layer⁴ or a tribo-chemical wear process.⁵ The goal of this work is to try to use some of these existing theories to understand the mechanisms of material removal in the MRF of glass.

Preston⁶ gave a classic theory of removal in glass polishing that is still being studied today. He states, “(. . .the rate at which material is removed) is proportional to the rate at which work is done on each unit area of the glass.” Furthermore, he defines the work done in time t as

$$w = \mu A p v t, \quad (1)$$

where w = work ($\text{N} \cdot \text{m}$), μ = coefficient of friction, A = area of contact between the glass and polishing lap (m^2), p = pressure applied to the glass part (N/m^2), v = relative velocity between the lap and the part (m/s), and t = time in which work is done (s).

The term μp is the specific traction, or drag divided by the contact area, of the polishing lap (felt in this case) on the glass. The expression in Eq. (1) states that the work done on the material is proportional to the specific drag force multiplied by the area of contact and the velocity. He continues to say that if the specific drag force remains constant, then the removal rate is proportional to “...the amount of felt that passes over it...this is independent of velocity, except in so far as velocity may affect the amount of felt passing over.”⁶ In general, these statements are true in MRF as well: namely, that the

material removal scales with the drag force and is primarily controlled by the time of contact between the abrasive and the glass surface.

Preston's equation is commonly written in a slightly different form,

$$\frac{dz}{dt} = C_P \frac{L}{A} \frac{ds}{dt}, \quad (2)$$

where dz/dt = the change in height in time, or removal rate (m/s), C_P = Preston's coefficient (m^2/N), L = total normal load applied (N), A = area over which wear occurs (m^2), and ds/dt = velocity of the work piece relative to the tool (m/s).

The difficulty comes in defining Preston's coefficient in Eq. (2). The discussion above shows that a friction coefficient makes up part of it, but several other things are accounted for in this coefficient. The importance of various effects that make up Preston's coefficient in MRF will be demonstrated here. One of these is the chemical effects associated with the presence of water in the MR fluid. The mechanics associated with how different abrasive types affect the removal of material in MRF are also given. Before describing the mechanisms of material removal in MRF, it is instructive to discuss proposed mechanisms in other polishing processes.

Review of Mechanisms of Material Removal

Silvernail and Goetzinger^{7,8} summarize various factors that are important to glass polishing. Aside from pressure and velocity, they note that the polishing agent, liquid carrier fluid, and polishing lap are all important. Their results show that adding water to the slurry dramatically increases the removal rate of a crown glass. They conclude that the improved removal rate due to the addition of water is independent of the other parameters in the system (e.g., abrasive concentration, pressure, etc.) and that the interaction is primarily with the glass. The results that show changes in the polishing due to lap type are inconclusive. An increase in removal rate is seen with an increase in cerium oxide content, showing that the concentration of the slurry is important to material removal. This effect generally levels off at a concentration between 10 wt% and 20 wt% (approximately 1 vol% to 3 vol%). Furthermore, they discuss how cerium oxide behaves as an excellent abrasive while other rare earth oxides that are similar in structure are not good abrasives. They cannot explain the increased polishing effect of cerium oxide.

Other authors describe glass material removal in terms of small fracture events caused by the abrasive interacting with the glass surface. Buijs and Korpel-Van Houten² describe material removal of glass surfaces by abrasive particles through an indentation fracture theory. This process is intended to explain lapping, but a polishing process based on a similar theory could be envisioned. Essentially they describe how the abrasive particle acts like a Vickers indenter under a normal load. Material removal occurs through lateral cracking of the glass under the indenter-like abrasive. Removal rates in this model depend on the shape of the particle and material properties of the glass (namely, elastic modulus, hardness, and fracture toughness). While this explanation is typically used to explain grinding and microgrinding, Lambropoulos *et al.*³ show that removal rates obtained with MRF correlate with the same material properties described by Buijs and Korpel-Van Houten. They explain the fracture occurring through mechanisms other than indentation, however. Asperities on the surface can be modeled as nanometer-sized cracks. The abrasive contacts the asperity through shear and normal loads. In this geometry, the shear load works to drive the crack, while the normal load tends to close the crack. If the shear force is large enough relative to the normal load, fracture of the asperity will occur. This is different from Buijs *et al.* in that this mechanism is shear driven, while their work is controlled by lateral cracking from normal loads indenting the particle. The work of Lambropoulos *et al.* is in its early stages, but it gives a plausible explanation of how removal rates in polishing correlate with parameters used to describe fracture.

Water's positive impact on polishing is discussed in several other references. If polishing is thought to consist of small fracture events, then the effect of water can be explained by Michalske and Bunker.⁹ The authors (and references) describe how water can attack the Si-O-Si bonds at the crack tip, which results in a reduced fracture toughness of the glass. Furthermore, the hydrolysis rate increases as the stress of the bond increases. Consider the model proposed by Lambropoulos *et al.*³ and/or Buijs *et al.*² According to Michalske and Bunker's theory, the presence of the water as well as the stresses applied by the abrasive to the glass surface would dramatically reduce the fracture toughness of the material as well as speed up the kinetics of the process.⁹ This possibly explains why water enhances the removal of glass in polishing.

A second, possibly related, mechanism of material removal also involves hydration of the glass surface due to chemical interaction between the carrier fluid (water) and the glass surface. Cook¹⁰ describes how the water molecule breaks Si-

O-Si bonds and how this helps to create a hydrated layer in the glass surface. Cumbo^{1,11} gives a summary of Cook's work and extends it with a study of the chemical effects in polishing experiments. Cook's¹⁰ process basically describes how the loads applied to the surface by the abrasive promote diffusion of water into the silica network. As the water dissociates, it attacks the bonds within the network, weakening the structure. This promotes bond breakage and material removal. Cerium oxide and zirconia particles are described as having "chemical tooth," which promotes bonding of the abrasive to the silica. This promotes material removal from the silica network as well as inhibits redeposition of material back onto the surface. For chemically inactive materials, such as diamond, removal is said to depend on the carrier fluid's ability to carry the removed material away since the silica does not bond with the abrasive.

Izumitani's theory of the mechanism of material removal is also based on the idea of the hydrated layer.⁴ This hydrated layer is caused by a chemical reaction between modifier ions in the glass and the hydrogen ions in the water. Material removal occurs by abrasive particles scratching away this layer. The speed at which material is removed depends on how quickly the hydrated layer is formed (chemical durability of the glass) and the hardness of the hydrated layer as well as the hardness and/or friability of the abrasive. He showed that a softer abrasive that is more easily crushed but still harder than the hydrated layer is most effective. His explanation is that the crushing provides more particles and therefore a higher frequency of scratching events. He also describes the necessary properties of the lap used in polishing. The lap must be hard enough to support the abrasive and transmit pressure, but soft enough to allow the particle to embed into the polishing lap.

Evidence in the literature supports the existence of a surface layer that is created by hydration of the surface during polishing. Izumitani⁴ creates a hydrated layer by immersing the glass surfaces in 0.1 N solution of HCl. Subsequent Vickers microhardness tests show a reduction in microhardness of this layer with increased immersion time. Furthermore, he shows that the polishing rate increases as the microhardness of the hydrated layer decreases. Yokota *et al.*¹² use ellipsometry to show the existence of the hydrated layer after polishing. They demonstrate a reduction in refractive index in a small surface layer in glasses that are susceptible to chemical attack. The size of these layers is of the order of tens of nanometers deep. Glasses of interest to this work, borosilicate crown and silica, each reportedly have hydrated layers of approximately 40 nm with the polishing conditions studied. Maaza *et al.*¹³ use grazing-angle neutron reflectometry (GANR) to study the hydrated layer.

They also show evidence of a hydrated layer from the polishing process. The hydrated layer of their Borkron surfaces was approximately 5 nm (Borkron is a special borosilicate glass used for neutron optics applications¹³). It is 15 nm for the floated face of float glass and 40 nm for the nonfloated face. They also report on the existence of 2-nm cracks in the float glass from the polishing process. Yokota *et al.*¹² describe how some chemically resistant glasses like fused silica (FS), Vycor, and Pyrex actually show densification of the material in these layers. They explain this densification to be caused by high local pressures on the glass surface due to polishing. Shorey *et al.*¹⁴ provide more evidence of densification in fused silica by comparing numerical simulations with nanoindentation experiments. Densification apparently depends on the state of stress from both normal and shear loading.

Kaller^{5,15} describes a process he refers to as a tribo-chemical friction wear process. According to Kaller, the abrasive should be softer than the surface being polished, and the most important property of a polishing agent is its ability to "grip" the surface. He states that the most effective polishing abrasives (mostly cerium oxide and iron oxide) have a large number of lattice defects produced during manufacture, and it is the presence of these defects that promotes the gripping of the abrasive to the surface. He describes three steps: The first is intimate contact between polishing grains and the glass surface. This coupled with friction or shear forces promotes lattice deformation and partial removal of surface layers of the abrasive grain. Second, removal of these surface layers exposes ionic vacancies in the lattice, which bond with the glass. Finally, the continued motion of the polishing wheel produces continuous removal of glass. He continues his discussion to address how manufacturing methods can produce more, or fewer, lattice defects, as well as determine the primary crystallite size. Important additional lattice defects are created through (1) valance change of the oxide, (2) incorporation of metal ions or molecules into the lattice, and (3) quenching. Finally, he discusses how careful control of processing allows control of crystallite size, number of defects, and rubbing resistance. For a given process a particle could be manufactured with the appropriate number of lattice defects so that the abrasion resistance matches the process for which it is intended. In other words, a cerium oxide particle can be produced that will provide a low rubbing resistance (soft particle), which means low removal, but a high precision surface. A (hard) cerium oxide particle could also be produced to provide a high rubbing stress, which would give higher removal, but less precise (rougher) surfaces. He states that the first abrasive would be used in low shear to be most effective, but that the second one

would increase its effectiveness at very high shear, presumably due to the exposure of new lattice defects. His only discussion of a hydrated layer is to say that experiments that were supposed to prove the existence of the hydrated layer did not. To explain other observations of a densified surface layer resulting from the pressure of polishing, Kaller claims evidence for nanometer-scale abrasive particles left on or in the surface after polishing. He refutes the idea of a smallest-size limit in milling of abrasives.

Kaller's ideas are at least partially supported by Kirk and Wood.¹⁶ In their paper, they describe the calcination of cerium oxide sol-gels and show evidence of significant changes in the crystallography due to calcination temperature. Before calcination, the particles are loosely bonded and of the order of 5 to 10 nm in size. After calcination at 850°C for 1800 s, the crystallite size increases to about 60 to 80 nm, and they become strongly bonded together. Furthermore, they show that the {111}-type planes grow faster than {200} planes at elevated temperatures. The {111} planes have a higher atom density than the {200} planes, which means that more cerium atoms are exposed. The hypothesis is that this explains the increased polishing efficiency of properly calcined cerium oxide.

Several views on the roles of the various constituents in the polishing process clearly exist. Water plays a major role in glass polishing. It is not clear whether this is due to the reduced fracture toughness at the glass surface or a softening due to chemical attack of the silica network. Actually, each process description is similar, and there may be two ways of saying the same thing. The type of abrasive is also important. The wide acceptance of cerium oxide in glass polishing is explained to be due to its chemical tooth, which could be explained by Kaller's lattice defect theory. Also, both Izumitani⁴ and Kaller⁵ show that it is possible to polish hard materials with relatively soft abrasives; however, hard materials such as diamond can also be used. The relative effectiveness of an abrasive is not solely due to its hardness.

Much of this discussion is as appropriate for MRF as it is for the more common pitch or pad polishing. The ability of abrasives softer than the glass to polish, even in the absence of water, will be shown. Furthermore, without water, abrasives harder than the glass surface have difficulty maintaining contact with the surface and actually have a lower material removal rate than the softer abrasive. This will be explained the same way Preston did for Eq. (1); namely, removal rate is proportional to how long the abrasive is in contact with the glass surface. The importance of water in MRF and how it

allows abrasives to more easily abrade material away from the surface will be shown. Finally, the interactions of different abrasives with the glass surface are demonstrated. An increase in abrasive concentration increases the time the abrasives are in contact with the glass surface. This results in increased removal. The hypothesis that cerium oxide grips the glass better and that this leads to an increase in measured drag force under identical experimental conditions as aluminum oxide and diamond is experimentally substantiated. Diamond drastically reduces drag but gives an increased removal rate.

Overview of MRF

Several references describe the evolution of MRF in recent years.^{17–19} This process utilizes magnetic particles, nonmagnetic polishing abrasives in either an aqueous or nonaqueous carrier fluid, and a magnetic field to polish materials. The “standard” MR fluid consists of 36 vol% of carbonyl iron (CI) as the magnetic component and 6 vol% of cerium oxide as the abrasive with the balance made up of de-ionized (DI) water and fluid stabilizers.^{19,20} Figure 83.43 shows an SEM and size distributions of particles after being used in MRF for one week. The dark spherical particles are the magnetic CI and have a median particle size of 4.5 μm . The lighter, small particles are the nonmagnetic abrasive, which in this case is cerium oxide. The cerium oxide starts with a median size of 3.5 μm with a fairly broad distribution. The SEM shows several significantly smaller particles that are likely due to milling of the abrasives during use. Proper manipulation and control of the MR fluid allows MRF to successfully polish a wide variety of materials with commercially viable removal rates.^{18,19} Removal rates obtained with the standard MR fluid vary from about 2 $\mu\text{m}/\text{min}$ for a hard silica glass like fused silica to more than 9 $\mu\text{m}/\text{min}$ for a soft laser glass like LHG8.¹⁷

The primary concern of this work is to study how MRF polishes glass. Figure 83.44(a) shows a photo of an MRF machine with a vertical wheel [schematic of this machine shown in Fig. 83.44(b)]. MR fluid is pumped from the fluid conditioner (1) up to the nozzle (2), where it is ejected onto the rotating vertical wheel as a ribbon. The wheel shape is that of a portion of a 150-mm-diam sphere. At the initial point of contact, the MR fluid is a viscous fluid with the approximate consistency of honey (viscosity $\approx 0.5 \text{ Pa}\cdot\text{s}$, yield stress $\approx 0 \text{ kPa}$). The rotation of the wheel drags the fluid under the part in region (3), where it is acted upon by the magnetic field. The MR fluid ribbon flows through the converging gap between the lens and the wheel. The magnetic field stiffens the ribbon in this region, giving it the approximate consistency of clay (yield stress $\approx 10 \text{ kPa}$). Significant forces are created by the interac-

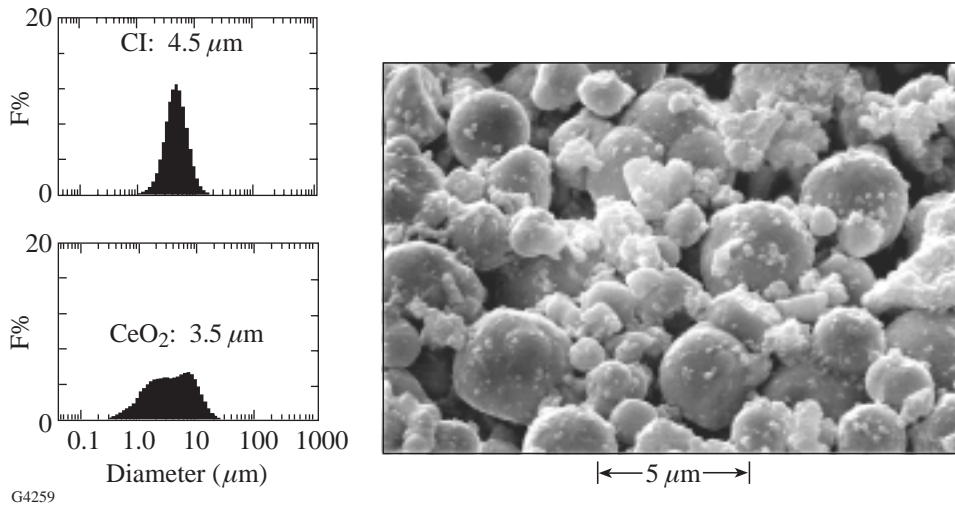


Figure 83.43 SEM of particles and their initial size distributions after one week of use in MRF. The dark spherical particles are the hard magnetic carbonyl iron particles. They have a median size of 4.5 μm. The smaller, light particles are the cerium oxide abrasives. They initially have a broad size distribution with a median particle size of 3.5 μm. The large amount of small particles in the SEM suggests that milling of the cerium oxide occurs during use.

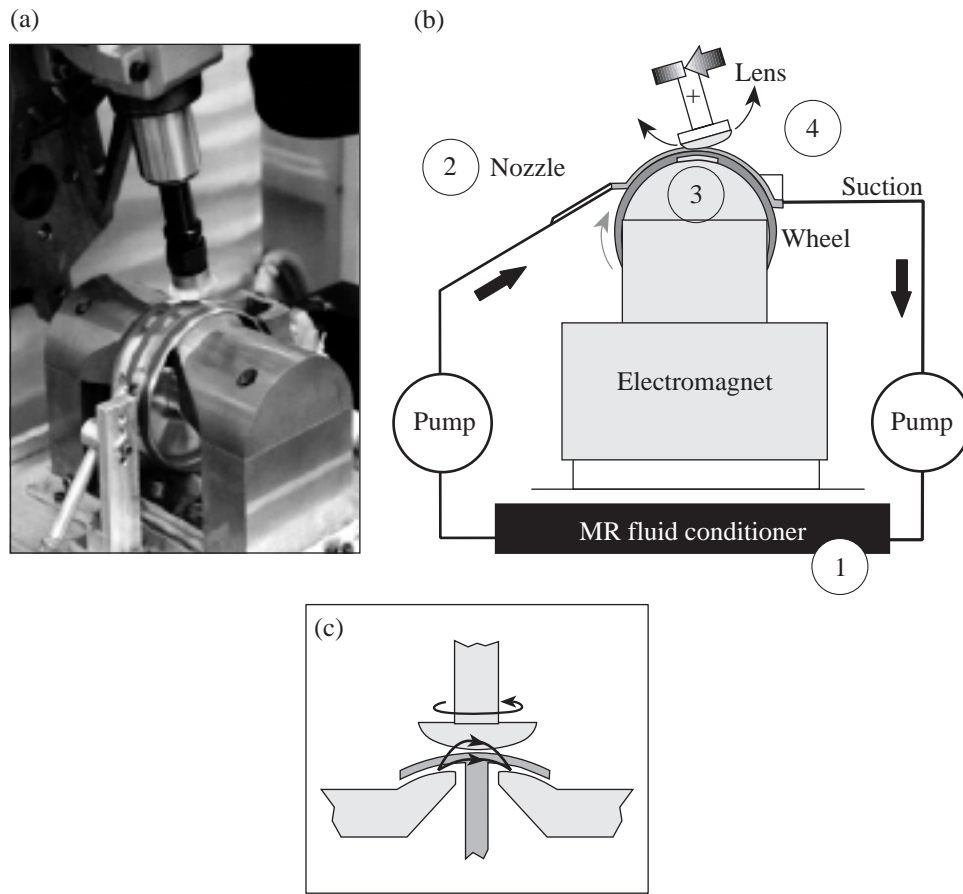


Figure 83.44 The setup used in MRF with a vertical wheel. (a) A photo of an actual MRF machine. (b) A schematic of the MRF machine. Fluid is pumped from the conditioner at (1) to the nozzle at (2) onto the rotating wheel. The wheel carries the fluid between the part and wheel into the magnetic field at (3), where the field causes it to stiffen. Hydrodynamic flow in this region causes stresses sufficient to cause removal to occur. The wheel continues to carry the fluid outside of the field region, where it is removed from the wheel at (4). This fluid is again pumped to the conditioner to complete the circuit. (c) Cross-sectional view showing the relative orientation of the 150-mm-diam spherical MRF wheel, pole pieces, and part. Field lines in the polishing zone are schematically shown.

tion between the wheel, MR fluid, and glass surface since the MR fluid ribbon flows through a converging gap, deforming from a thickness of 2 mm to one of 1.5 mm. Rotation of the wheel continues to drag the MR fluid from region (3) over to region (4), where it is removed from the wheel through suction. Here, the magnetic field does not act on the MR fluid, so it again has the consistency of honey. The MR fluid is pumped back to the fluid conditioner, where it is cooled to a setpoint temperature and any evaporative losses are replaced. Our primary area of concern is region (3) inside the magnetic field where polishing occurs. Figure 83.44(c) shows a cross-sectional view of this region. The pole pieces provide the magnetic field to stiffen the MR fluid. This fringing field between the gap of the pole pieces has a strong vertical gradient. The field is higher at the wheel surface than it is at the part surface, which causes the CI to be pressed against the wheel surface and the nonmagnetic abrasive to move to the glass surface.

Figure 83.45(a) shows a photo of the MR fluid contacting a meniscus lens surface (flow direction is left to right for all of Fig. 83.45). The fluid contacts the surface in the shape of a backward D. This is the shape of the removal under the action of the rotating wheel if the part is held stationary in the fluid. This D-shaped region is referred to as the “spot” from this point on. The white regions surrounding the spot and extending downstream (to the right) from the spot are abrasive particles. This is evidence of the fact that abrasives move to the part surface under the action of the magnetic field. Figure 83.45(b) shows an interferogram of a removal spot; its oblique view is shown in Fig. 83.45(c) (adapted from Ref. 18). The surface before and after a removal experiment is evaluated using a phase-shifting interferometer.²¹ The instrument software is used to subtract the initial surface from the final surface containing the spot. Height variations on the resulting image

are due to material removed from the initial surface. The peak removal rate is found by dividing the depth of deepest penetration by the contact time between the part and MR fluid ribbon.

The proximity of the part and wheel surface changes due to the curvature of the wheel (and part, if polishing a lens). The location of the deepest and widest part of the spot shown in this figure is approximately the position of closest approach between the part and the wheel surface. During polishing, the part is rotated and swept through the polishing zone, allowing material to be removed in annular regions over the entire part surface. Computer-controlled dwell times allow control of the surface figure of the polished surface to a precision of $\lambda/20$.¹⁸

Removal mechanisms on a macroscopic scale have been previously considered.^{22,23} Since the normal force on an abrasive particle is low compared with conventional polishing,²⁴ a shear-controlled mechanism has been described.^{22,23} MR fluids are modeled as Bingham fluids with a yield stress (~10 kPa) and small plastic viscosity (~0.5 Pa•s).^{17,22,23,25} The flow of a fluid with a yield stress through a converging gap, like the one between the rotating wheel and part surface in MRF, allows the possible formation of unsheared regions called “cores” (see Fig. 83.46). These cores effectively reduce the gap between the wheel and part surface and cause increased shear stresses on the downstream end of flow. While the opacity of the MR fluid prevents visual confirmation of the presence of these cores, material removal has been shown to increase in the region where these cores are expected to be located.²³ In general, the low normal loading in MRF keeps an abrasive particle in contact with the glass surface, but material removal is primarily controlled by the shear stresses applied to the abrasive through the bulk flow of the MR fluid.

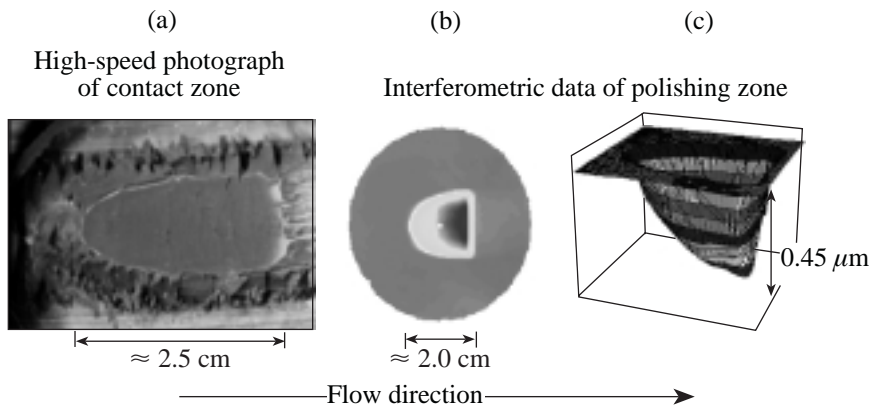


Figure 83.45

The spot in MRF. Flow is from left to right in all parts of this figure. (a) An actual photo of the contact region, or “spot,” on a stationary meniscus lens. (b) Interferogram of the material removed from the spot. Interferometric characterization of the spot gives a removal function that a computer program can use to vary dwell time of this spot over the surface. This allows precise control of the figure during polishing. (c) An oblique view of the figure during polishing. The deepest region is at the trailing edge of the flow and is approximately the position of closest approach between the part and wheel.

G4996

Experimental Considerations and Earlier Screening Studies

The spot-taking machine (STM)—a machine similar to the commercial MRF polishing machine²⁶—is used to perform these material removal experiments [see Fig. 83.44(a)].¹⁹ The only automated degree of freedom in the part motion on the STM is the height of the part above the rotating wheel. There is no rotation or swing of the part, so a removal experiment consists simply of making a spot on a flat part. Important machine parameters are held constant for all removal experiments. The vertical wheel rotates at 150 rpm, the MR fluid ribbon height is 2.0 mm, and the part surface is placed 0.5 mm into the MR fluid. The current to the electromagnet is kept at 15 A. This results in the magnetic flux density having a horizontal component of about 260 kA/m, 1 mm above the wheel surface.²⁷

Water loss due to evaporation from aqueous MR fluids is a concern during removal experiments. If this evaporation is left unchecked, the actual CI concentration of the MR fluids, and therefore the viscosity and yield stress, will increase. The STM monitors the viscosity in real time and maintains the appropriate CI concentration. An off-line moisture analyzer is used at the beginning of each experiment to measure moisture content in the MR fluid.²⁸ It is therefore possible to calculate the actual CI concentration for data analysis.

The viscosity outside of the magnetic field is measured off-line before each set of experiments using a cone and plate viscometer²⁹ whose shear rate may be varied from 0 to 960 1/s. These MR fluids are shear thinning, which means that the apparent viscosity decreases as the shear rate increases. Because of this, the viscosity is monitored at only the maximum shear rate since this is the approximate shear rate both in the fluid delivery system and underneath the part during polishing.

For all the experiments performed, the viscosity at 960 1/s is 60 ± 20 cps. As expected, the viscosity tends to increase with the amount of solids in an MR fluid. This viscosity is kept low so that it is easily pumped by the fluid delivery system.

Roughness measurements are made with two instruments. One is a white-light interferometer, which measures the roughness over a $0.25\text{-mm} \times 0.35\text{-mm}$ area and has a lateral resolution of $1.1 \mu\text{m}$.³⁰ This interferometer is a valuable tool in measuring the microroughness of a part. The second instrument is an atomic force microscope (AFM), which measures the roughness over a smaller region.³¹ Scans are performed in contact mode over a $5\text{-}\mu\text{m} \times 5\text{-}\mu\text{m}$ -square region using 256 samples, at a rate of 1 Hz. This allows us to investigate submicron features from polishing with a lateral resolution approaching 20 nm. The vertical scale is 15 nm for all AFM scans presented here.

Each fluid is characterized on the magnetorheometer described in previous work^{23,25} to determine the dynamic yield stress of the fluid. The MR fluids are tested at magnetic fields with flux densities of 200 kA/m and 250 kA/m only, since this is the nominal flux density at 15 A on the STM in the region of fluid/part interaction. Fixed conditions for other experimental parameters on the magnetorheometer are polishing configuration, 0.5-mm gap, and 3.33-rpm cup speed. The results of our work on the magnetorheometer are shown in Fig. 83.47. The data from this experiment were taken in the range of 40 vol% to 45 vol% CI. The dynamic yield stress does not change for CI compositions greater than about 35 vol% CI but asymptotically approach values of about 15 kPa at 200 kA/m and 20 kPa at 250 kA/m for a variety of commercial CI powders. The yield stress of the MR fluid is also unaffected by the incorporation of nonmagnetic abrasives at the low loading used for these experiments.

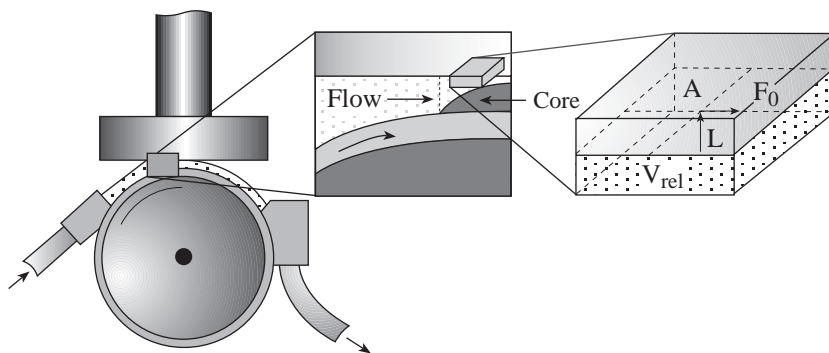


Figure 83.46 Schematic showing the contact between the MR fluid and the glass. The first callout shows the internal structure of the flow. The removal rate increases in the region of the core due to the increased shear stresses that result from the throttling action of the core. If material removal is considered over a small material volume, a Preston-type equation based on the shear stress at the part surface can be used to describe the removal process.

G4997

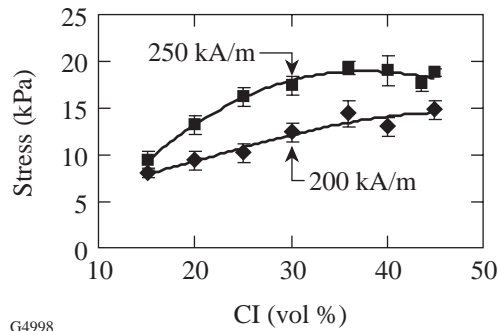


Figure 83.47

Dynamic yield stress measured on the magnetorheometer for the MR fluids used in removal experiments. Measurements were taken in the polishing configuration, 0.5-mm gap and 3.33-rpm cup speed at fields with a flux density of 200 kA/m and 250 kA/m. The yield stress is approximately 15 kPa at 200 kA/m and 20 kPa at 250 kA/m for the fluids between 40% and 45% CI concentration—the region of interest for these experiments. This data is for a variety of CI types, both with and without abrasives. The type of CI and presence of abrasives in this low loading have no effect on the dynamic yield stress of the MR fluid. Solid lines have been added only to aid the eye.

The flow of an MR fluid between the part surface and wheel is complicated. The yield stress does not give a full representation of the forces applied to the part by the fluid during removal.^{22,23} Because of this, the pressure and the total drag force applied to the part by the fluid are measured as well. A pressure-sensing pad³² is used to measure the pressure distribution applied to the part by the MR fluid. Measurements are taken by adhering the sensor to the part surface and lowering it into the MR fluid ribbon.

The drag force is measured using a linear translation stage,³³ a sapphire flat, and a 5-lb (≈ 22.2 N) load cell.³⁴ The interaction between the sapphire flat and the MR fluid forces the linear stage in the direction of flow. The linear stage, free to move horizontally, is driven into the load cell with a force equal to the drag force applied by the MR fluid. Drag force measurements are taken with the part at a depth of 0.5 mm into the MR fluid for experiments with nonaqueous MR fluids and a 1.0-mm depth with aqueous MR fluids (drag force measurements reported later for aqueous MR fluids without abrasives were done at both 0.5-mm and 1.0-mm depths). While this does not allow a direct comparison between pressure and drag measurements, it is sufficient for an evaluation of the relative performance of each fluid where the pressure and drag force are considered separately.

To fully understand mechanisms of material removal in MRF, the roles of the various constituents of the MR fluid need

to be separated and evaluated. In previous work, we described how the nanohardness (H_{nano}) of the magnetic carbonyl iron (CI) and nonmagnetic polishing abrasives could be determined through novel nanoindentation techniques.^{35,36} These results were used to conduct initial screening experiments on the importance of (1) the nanohardness of the CI in nonaqueous MR fluids without abrasives and (2) the effect of gradually adding DI water to the MR fluid and how the DI water changed abrasive interactions with the glass surface.³⁶ It was found that in nonaqueous MR fluids, CI that was softer than the glass surface slowly abraded material but did not penetrate the glass surface. Harder CI penetrated the glass surface. Adding DI water turned on chemistry and changed the way hard particles were seen to interact with the glass surface, due to the evolution of a hydrated or underdense (corroded) layer that enhanced rates of material removal. Removal rates were related to the mechanical properties of the CI and the glass. Surface morphologies resulting from abrasive/part interaction were consistent for three different glass types: BK7, LHG8, and FS.

Mechanisms of Removal in MRF

The work described in this section is based upon our previous screening studies. Aqueous MR fluids are used to remove material from a fused-silica (FS)³⁷ surface. These MR fluids are made up separately of hard CI ($H_{\text{nano}} = 11.7 \pm 0.8$ GPa), soft CI ($H_{\text{nano}} = 2.2 \pm 1.0$ GPa), and varying amounts of nonmagnetic polishing nano-abrasives (cerium oxide, aluminum oxide, and diamond). Variations in the material removal of FS ($H_{\text{nano}} = 9.9 \pm 0.1$ GPa) are monitored as a function of abrasive type and amount.

To study the effects of DI water in polishing requires a carrier fluid that suppresses the chemical effects. A dicarboxylic acid ester (DAE) has a density of 1.189 g/ml at 20°C³⁸ and a viscosity of 2.85 cps at 23°C,³⁹ which is similar to the density and viscosity of water, 0.982 g/ml and 1.0 cps, respectively.³⁸ This allows the nonaqueous DAE-based MR fluid to have a solids loading and rheology similar to the aqueous MR fluid. Another advantage of the DAE is that water is soluble up to 8.3 wt% (≈ 7 vol%), which makes it possible to study the chemical effects of water incrementally. Removal rates of BK7 glass were shown to increase exponentially with water concentration in this range (see Ref. 40).

The nine MR fluids studied here are summarized in Table 83.VIII. MR fluids 1 through 5 are made up with a carrier fluid and CI only. MR fluid 1 has 40 vol% soft CI and 60 vol% DAE; MR fluid 2 contains 40 vol% of the hard CI and 60 vol% DAE. MR fluid 3 is the same as MR fluid 2, except

that 1 vol% DI water is added to the composition. MR fluids 4 and 5 are the same as MR fluids 1 and 2 except that MR fluids 4 (soft CI) and 5 (hard CI) utilize an aqueous carrier fluid (made up of DI water and <1 vol% of stabilizing agents).

1. Removal Experiments Without Polishing Abrasives

Each MR fluid was used on the STM to put a removal spot on a 50-mm-diam FS surface initially polished flat to within $\lambda/4^{21}$ and 0.9 ± 0.1 -nm rms roughness.³⁰ Normal stresses were measured as previously described. The peak pressure was found to be 129 ± 4 kPa for all tests. The drag force was measured at a 0.5-mm gap and found to be 0.6 ± 0.2 N. This 0.2-N variation is measured within three repetitions of a single experiment and is due to the resolution of the cell. Removal rates were determined interferometrically as described on p. 162. Stated removal rates are the peak removal rate for a single spot. Removal rates under identical conditions in MRF have been found to be repeatable to within 2.5% error.²³

The results of this study are shown in Fig. 83.48. The areal rms roughness is plotted against the peak removal rate with the profilometer maps³⁰ given. The number on each profilometer map corresponds with the MR fluid number of the experiment, and the arrow gives the flow direction of the MR fluid. MR fluid 1, with soft CI, gives a low removal rate of $0.003 \mu\text{m}/\text{min}$

and a relatively low roughness (2.3 ± 0.1 nm) and leaves faint grooves in the direction of flow. No sleeks are apparent (sleeks are defined as the pit-like features with comet tails). The removal rate is still low for MR fluid 2 ($0.004 \mu\text{m}/\text{min}$) but the areal rms roughness increases to 22.6 ± 1.7 nm. Large numbers of pits and sleeks are seen as a result of the hard CI. The effect of adding a small amount of water to MR fluid 2 is shown with the result for MR fluid 3. The removal rate increases $2.5 \times$ to $0.010 \mu\text{m}/\text{min}$, and the areal roughness drops to 7.0 ± 1.0 nm rms. Also, the numbers of sleeks is reduced, and they tend to become longer scratches. Using MR fluids 4 and 5 for removal experiments further emphasizes the effect of the DI water. The removal rate increases from $0.01 \mu\text{m}/\text{min}$ (MR fluid 3) to $0.23 \mu\text{m}/\text{min}$ for MR fluid 4 and $0.14 \mu\text{m}/\text{min}$ for MR fluid 5. The $0.25\text{-mm} \times 0.35\text{-mm}$ areal rms roughness values for these two aqueous MR fluids are greatly reduced (0.8 ± 0.2 nm for MR fluid 4, and 1.3 ± 0.3 for MR fluid 5). Also, the profilometer scans clearly indicate many fewer sleeks than for the nonaqueous MR fluids. It is interesting to note that the soft CI-based MR fluid 4 actually has a higher removal rate than the hard CI-based MR fluid 5. Otherwise, the presence of the DI water significantly diminishes the effect of the CI particle hardness in these experiments. Atomic force microscope images over $5\text{-}\mu\text{m} \times 5\text{-}\mu\text{m}$ areas show no significant differences in the FS surface for removal experiments with MR fluids 4 or 5.

Table 83.VIII: Summary of the MR fluids used for material removal experiments.

MR Fluid Number	Vol% CI	†CI Nanohardness (Gpa)	DAE (Vol%)	*Water (Vol%)	Abrasive Type (Amount, Vol%)
1	40	2.2 ± 1.0	60	0	None
2	40	11.7 ± 0.8	60	0	None
3	40	11.7 ± 0.8	59	1	None
4	40	2.2 ± 1.0	0	60	None
5	40	11.7 ± 0.8	0	60	None
6	40–45	11.7 ± 0.8	0	Balance	Cerium oxide (0–1.0)
7	40–45	11.7 ± 0.8	0	Balance	Aluminum oxide (0–1.0)
8	40–45	11.7 ± 0.8	0	Balance	Diamond (0–0.1)
9	40–45	2.2 ± 1.0	0	Balance	Cerium oxide (0–1.0)

*Aqueous MR fluids contain DI water and <1 vol% fluid stabilizers.

†Hardness measured with nanoindentation at 1 and 5 mN; FS nanohardness is 9.9 ± 0.1 Gpa at these loads.^{35,36}

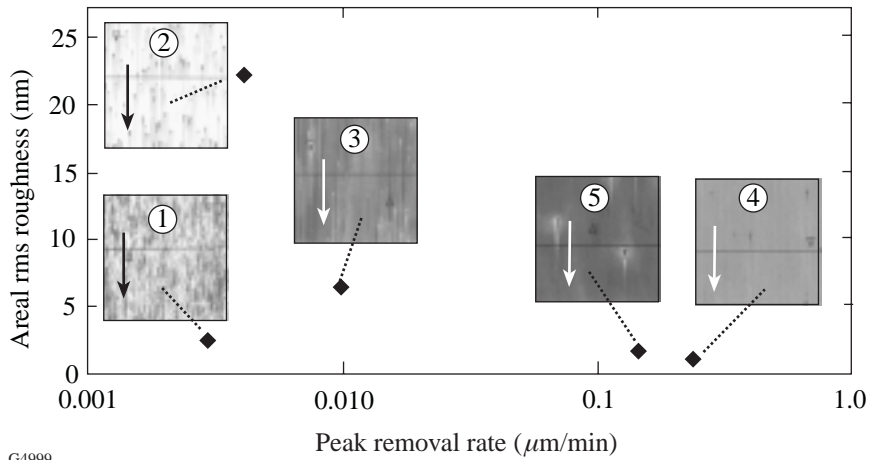


Figure 83.48

Areal ($0.25\text{-mm} \times 0.35\text{-mm}$) rms roughness versus peak removal rate on FS for MR fluids 1 through 5. The soft CI (MR fluid 1) is able to remove material at a very low rate in the absence of the chemical effects of water, but does not pit the surface. The hard CI without water (MR fluid 2) gives low removal and high roughness as the hard CI leaves pits and sleeks in the softer FS surface. The addition of 1 vol% DI water to MR fluid 3 decreases the number of sleeks, which results in a decrease in roughness, and increases removal rate. Fully aqueous MR fluids 4 and 5 show a decrease in pits and sleeks, decrease in roughness, and dramatic increase in removal rate.

G4999

2. Removal Experiments with 40 vol% to 45 vol% CI and Nonmagnetic Nano-Abrasives

Table 83.VIII also lists the composition information for MR fluids 6 through 9. The same hard and soft CI powders that were used in the previous experiments are used here. Table 83.IX summarizes the properties of three different types of nonmagnetic abrasives used in combination with the CI's. These abrasives are nano-cerium oxide,⁴¹ nano-aluminum oxide,⁴² and nano-polycrystalline diamonds.⁴³ The cerium oxide and aluminum oxide abrasives are described in the product literature⁴⁴ as loosely bound agglomerates approximately $10\ \mu\text{m}$ in size. It should be possible to disperse them down to agglomerates of a few hundred nanometers with moderate milling. Cerium oxide from an MR fluid was recently sized after being used in the STM. The mean diameter of the cerium oxide used for 10 days was found to be $0.125\ \mu\text{m}$ and that used for only 2 h was $>0.3\ \mu\text{m}$.⁴⁵ The milling that occurs in the STM among these particles and the CI breaks up any loose agglomerates. The stated primary particle sizes are 37 nm for the alumina and 11 nm for the cerium oxide.^{44,46} The polycrystalline diamonds have a particle size of about $0.125\ \mu\text{m}$ and are made up of crystals approximately 10 nm in size.⁴⁷ The advantage of using these nanoabrasives is that their particle sizes are similar, and they can be introduced in small quantities to the aqueous MR fluid without causing large changes in MR fluid rheology.

Notice from Table 83.VIII that the cerium oxide and aluminum oxide are added in concentrations ranging from 0 vol% to 1.0 vol%, while the diamonds are added in a volume loading up to only 0.1 vol%. This is due to the fact that the diamonds have an immediate and dramatic effect, whereas the other, softer abrasives have a more gradual effect. Also, due to the high cost of diamonds ($\approx \$10/\text{gram}$ versus $\approx \$0.10/\text{gram}$ for cerium oxide), their addition into the MR fluid was halted as soon as

the removal rate appeared to be unaffected by the addition of more diamonds. The difference in the performance of these abrasives is found to be significant even in the small volume loadings given here.

The next step in these experiments is to gradually add the nonmagnetic abrasives into the MR fluid. Figure 83.49 shows the removal rate for FS as a function of cerium oxide concentration for experiments done with MR fluid 6 at a 45 vol% hard CI concentration. The $5\text{-}\mu\text{m} \times 5\text{-}\mu\text{m}$ AFM scans representative of the FS surface at a given concentration of cerium oxide and their cross-sectional profiles are also given in this figure. The 15-nm scale length given in Fig. 83.49 (and Fig. 83.50) is appropriate for each profile in the figure. The AFM scans are shown because their lateral resolution (approximately 20 nm) allows for better characterization of an abrasive's performance than the $0.25\text{-mm} \times 0.35\text{-mm}$ profilometer maps do (lateral resolution = $1.1\ \mu\text{m}$). The white arrows in these AFM scans indicate the direction of flow. The removal rate increases from $0.62\ \mu\text{m}/\text{min}$ with no cerium oxide to $0.94\ \mu\text{m}/\text{min}$ with only 0.05 vol% cerium oxide. Distinct scratches caused by the small amount of cerium oxide in the MR fluid become apparent. The removal rate climbs to $3.01\ \mu\text{m}/\text{min}$ when the cerium oxide concentration is increased 10 \times to 0.5 vol% cerium oxide. The removal rate increases further, to $3.51\ \mu\text{m}/\text{min}$, as the cerium oxide concentration is increased to 1.0 vol%. The areal rms is $0.9 \pm 0.1\ \text{nm}$ for the scans in this figure. It is clear that not only does the cerium oxide become responsible for material removal but also a change in the surface morphology becomes apparent. These scans give more evidence that cerium oxide moves into the layer between the CI and the glass surface and becomes the primary agent for material removal. When cerium oxide is added to the MR fluid, the CI particle is no longer a primary abrasive. The increase in the number of polishing

grooves or scratches caused by the increase in nonmagnetic abrasive concentration is seen for all three types of nonmagnetic abrasives.

Additional information can be gained by considering the differences in morphology of the FS surfaces for the different abrasives used in polishing. Figure 83.50 shows the removal rates from experiments using the MR fluids with 45 vol% hard CI and the maximum loading of the three nano-abrasives used

for these experiments. The lowest removal rate here ($0.62 \mu\text{m}/\text{min}$) is for the MR fluid without nonmagnetic abrasives. When 1.0 vol% aluminum oxide is added, the removal rate increases to $1.0 \mu\text{m}/\text{min}$. Removal rates are even higher for the other nonmagnetic abrasives: $3.51 \mu\text{m}/\text{min}$ for 1.0 vol% cerium oxide, and $4.66 \mu\text{m}/\text{min}$ for 0.1 vol% diamond. An examination of the $5\text{-}\mu\text{m} \times 5\text{-}\mu\text{m}$ AFM maps in Fig. 83.50 shows differences in how these three nonmagnetic abrasives interact with the glass surface. The scan for the MR fluid with 45 vol%

Table 83.IX: Summary of particle size information for the nano-abrasives used.

	Primary Particle Size (nm)	Aggregate Size (μm)	Agglomerate Size (μm)
Cerium Oxide	11	1.5	3.0
Alumina	37	0.3	N/A
Diamond	10	0.125	N/A

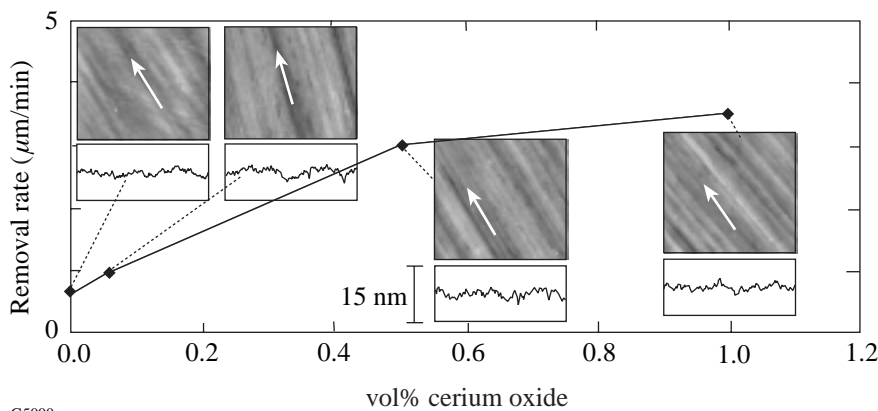


Figure 83.49

Removal rate versus concentration of cerium oxide for experiments using MR fluid 6 (each MR fluid contained 45 vol% hard CI and the aqueous carrier fluid). The removal rate increases with cerium oxide concentration, leveling off at about $3 \mu\text{m}/\text{min}$. The inset AFM scans and accompanying profiles show evolution of the morphology of the FS surface as the abrasive is added. The cerium oxide moves to the interface between the CI and the glass to control removal. The 15-nm scale applies to all profile plots.

G5000

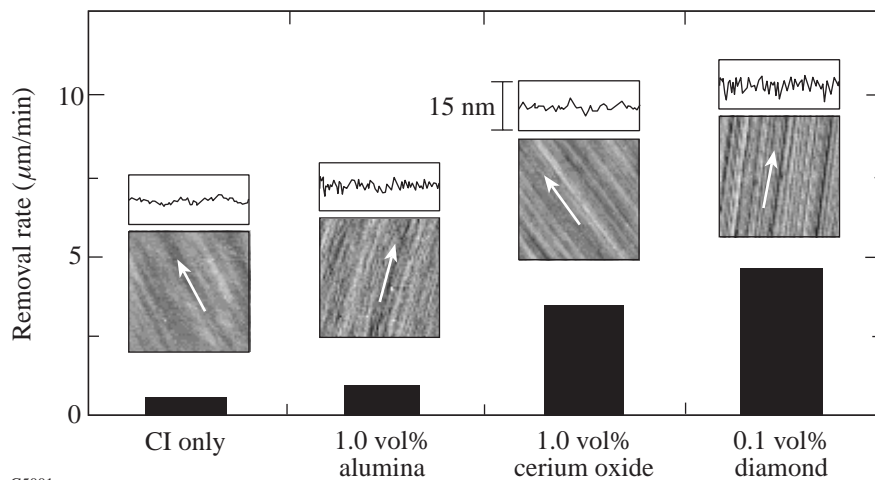


Figure 83.50

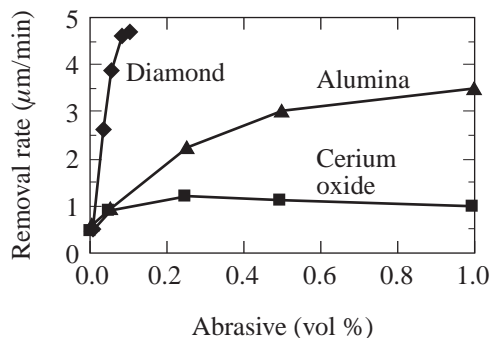
Removal rate as a function of abrasive type for MR fluids with 45 vol% hard CI and the maximum amount of abrasive used during these experiments (only up to 0.1 vol% diamond was used due to its high cost and high removal rates). The three abrasive types affect removal rates to varying degrees due to differences in how each interacts with the FS surface. Aluminum oxide gives deep ($\approx 4 \text{ nm}$) discontinuous grooves; cerium oxide gives shallower (≈ 1 to 2 nm), continuous grooves; and diamond gives deep ($\approx 4 \text{ nm}$) continuous grooves in the direction of flow. Characteristics of the polishing grooves help explain differences in removal rates for the three types of nano-abrasives.

G5001

hard CI without nonmagnetic abrasives is the same scan shown in Fig. 83.49. It has an areal rms of 0.8 nm. The aluminum oxide does not appear to continuously scratch the surface; instead, there appear to be several small discontinuous scratches at the FS surface. This leads to the lowest removal rates for the MR fluids containing nonmagnetic abrasives and an areal rms roughness of 1.2 nm. The cerium oxide gives wide, continuous scratches over the scanned region and an rms roughness of 0.9 nm. Finally, the diamond gives distinct narrow, continuous scratches along the direction of flow. The areal rms roughness for this scan is 1.4 nm. More differences in the behaviors of the abrasives are observed and are discussed below.

Differences in the Mechanics of Removal for Aqueous MR Fluids

Figure 83.51 shows the removal rate for MR fluids made up of 45 vol% hard CI and increasing amounts of nonmagnetic abrasives. Small amounts of diamond cause dramatic increases in removal rates. Cerium oxide increases removal to a lesser degree, and the aluminum oxide increases removal to an even lesser degree. These removal rates tend to level off at higher nonmagnetic abrasive concentrations. A certain minimum amount of nonmagnetic abrasive is needed to maximize the effectiveness, but there is a point where the addition of more abrasive has little or no effect on the removal rate. This has been shown to be true in more conventional polishing methods as well. Izumitani⁴ showed a maximum in polishing efficiency of BK7 glass at about 1.5 vol% (10 wt%) cerium oxide. It is not clear whether this polishing was done on pitch or on a polyure-



G5002

Figure 83.51

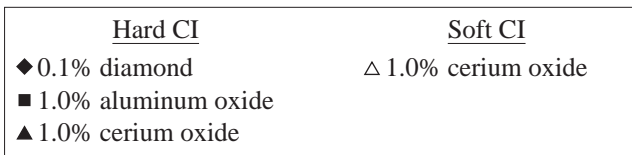
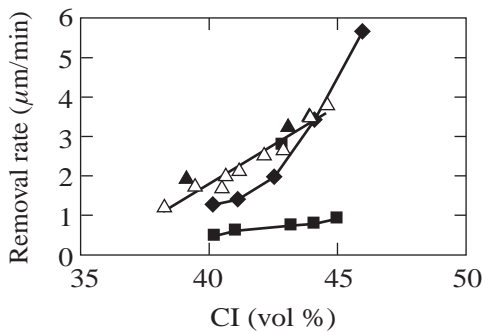
Removal rate versus vol% abrasive for 45 vol% hard CI and the aqueous carrier fluid. The diamonds are shown to have an immediate impact, dramatically increasing removal with less than 0.1 vol% concentration. The cerium oxide gradually increases removal. The aluminum oxide proves ineffective at increasing removal rates.

thane lap. Silvernail and Goetzinger⁸ show similar behavior on felt and Pellon laps. Their result depends on the applied pressure, but most of their removal rates level off above 1.5 vol% cerium oxide. Presumably this means that once the contact zone between the CI and the glass surface is saturated with nonmagnetic abrasive, further addition of abrasives is unnecessary.

The reason for the relative effectiveness of each particle type is not clear, but these results do agree with AFM measurements as well as with the experiments with nonaqueous MR fluids. The cerium oxide grooves are approximately 1 nm to 2 nm deep, whereas the aluminum oxide and diamond grooves are approximately 4 nm deep.⁴⁰ The diamonds, the hardest particles, exhibit distinct continuous scratches, which leads to high removal rates. The cerium oxide also scratches the material in a continuous manner, but the scratches are less severe, which leads to an intermediate removal rate. The lowest removal rate is for the aluminum oxide particles, even though they give features deeper than those from cerium oxide and as deep as those from diamond. The scratches associated with these aluminum oxide particles are discontinuous. The relative hardness values of the aluminum oxide and cerium oxide particles are not known because these particles are too small for nanoindentation experiments. Nanohardness tests done in a previous work³⁵ showed that it is possible for an aluminum oxide particle to be either very much harder than a cerium oxide particle or of comparable hardness. Even if the relative hardness values are not known, however, differences in removal rates should not be surprising after viewing the AFM scans. The continuity of contact between the abrasives and glass surface is important for high removal rates.⁶ The diamond and cerium oxide have this continuous contact while the aluminum oxide does not. The previous study³⁶ with the nonaqueous MR fluids without nonmagnetic abrasives (MR fluids 1 and 2) gave a similar result. The soft CI removed material from BK7 and LHG8 more efficiently than the hard CI. This trend changed somewhat when FS was used, probably because removal rates were so low and the hardness of FS is nearly the same as the hard CI. The proposed phenomenological explanation was that the soft CI could not penetrate the surface and was able to maintain contact with a shallow surface layer. The hard CI gave sleeks and pits and seemed to “skip” along the surface, causing discontinuity of contact between the abrasive and the glass surface. The reduced removal rate for aluminum oxide caused by discontinuity of abrasive/glass contact is consistent with these results. This may also be a partial explanation as to why Kaller¹⁵ recommends abrasives that are softer than the bulk material and Izumitani⁴ recommends abrasives with the same hardness of the hydrated layer.

Several references support these relative removal rates. The aqueous MR fluids have an approximate pH of 9. In Ref. 10 Cook analyzes work from others that shows cerium oxide is a much more efficient polisher than aluminum oxide in the pH range of 7 to 9. Cumbo¹¹ shows that cerium oxide has a higher removal rate on FS than aluminum oxide on FS at pH 10. Kaller and Cook give possible explanations for the effectiveness of cerium oxide. Kaller¹⁵ explains that lattice defects in cerium oxide crystals allow cerium oxide to grip the material better and therefore enhance removal rates. Cook's¹⁰ explanation is that the near neutral charge on the cerium oxide surface at this pH improves its ion exchange ability. The increased removal rate for diamond could be due to similar reasons. Its high hardness gives an explanation for the deep, distinct polishing grooves. The continuous contact maintained by the diamond could be explained by the fact that these diamonds are created by an explosion process,⁴⁷ which would likely result in many lattice defects. Kaller's explanation for cerium oxide provides support for the efficient removal seen with the MR fluids with diamond abrasives.

Figure 83.52 shows the removal rate as a function of CI concentration at the maximum nonmagnetic abrasive concentrations for the three abrasives used during these experiments. Notice that the data for MR fluids 6 (hard CI and cerium oxide)



G5003

Figure 83.52 Effect of the CI concentration on removal with maximum amount of abrasive present. Once again the diamonds prove to be the most efficient, reacting strongest to the increase in CI concentration. The cerium oxide data consist of both hard and soft CI. This shows that the hardness of CI is unimportant in the presence of the abrasive.

and 9 (soft CI and cerium oxide) coincide. This is more evidence that the type of CI is unimportant in aqueous environments with nonmagnetic abrasives, when the CI acts only as a lap. This plot shows the general trend that an increase in CI concentration leads to higher removal rates and that the relative increase in removal rate is largely related to the abrasive type. The nonmagnetic abrasives efficiently increase removal rate and decrease roughness. The diamonds are 10× more efficient than cerium oxide and aluminum oxide.

Figure 83.53 shows how the removal rate changes with pressure and drag force (pressure and drag force changed as a result of varying CI concentration but keeping the nonmagnetic abrasive concentration and wheel velocity constant). Figure 83.53(a) shows the removal rate as a function of drag force at the maximum nonmagnetic abrasive concentration used for these experiments. Figure 83.53(b) shows the removal rate as a function of the peak pressure. Both drag force and pressure scale with removal rate in a linear way, which is consistent with considerations such as Preston's equation⁶ discussed at the beginning of this article. The slopes of these lines (related to a Preston-type coefficient) depend on the type of abrasive used. The linear fits for the drag force tend to go through the origin, whereas they do not for the pressure. This supports the theory that in MRF the shear stress controls removal of material.

The drag force as a function of nonmagnetic abrasive content at a constant CI concentration is plotted in Fig. 83.54 for MR fluids 6, 7, and 8. As nonmagnetic abrasives are added, the drag force is reduced. This is once again consistent with the idea that nonmagnetic abrasives move to the region between the CI and the glass surface. All of the curves start at approximately the same initial drag force of about 5.5 N without nonmagnetic abrasive. While the MR fluid lap yields and conforms to the part surface, the magnetic field gives it a certain rigidity that makes it relatively difficult to shear. It is almost a two-body abrasion problem. This changes when nonmagnetic abrasives are added. They are forced to the glass surface because of the gradient in the magnetic field. At this point, the process becomes a three-body abrasion system. The magnetically stiffened CI forms the polishing lap that supports the free abrasives against the glass surface. This is similar to loose abrasive polishing on a conformal lap.

Consider the relative reductions in the drag force. The diamonds are seen to reduce the drag force dramatically, while increasing the removal rate just as dramatically. Adding aluminum oxide to the MR fluid also significantly reduces the drag

force, but adding cerium oxide has very little effect. This does not correlate with removal but may be interesting for a different reason. Several authors (see, for example, Refs. 10 and 15) hypothesize that one of the reasons cerium oxide is a successful polishing agent is because of its ability to chemically bond with the glass surface. This plot may begin to give physical evidence of this phenomenon.

All of these results suggest the use of a modified Preston equation to describe material removal in MRF. Consider Eq. (2). If a coefficient of friction is pulled out of C_p , it can be written as

$$\frac{dz}{dt} = C'_p \frac{\mu L}{A} \frac{ds}{dt} \tag{3}$$

The term C'_p is a new Preston coefficient and μ is a coefficient of friction. The friction coefficient multiplied by a normal load gives a drag force (F_D) and Eq. (3) becomes

$$\frac{dz}{dt} = C'_p \frac{F_D}{A} \frac{ds}{dt} \tag{4}$$

Finally, if this is considered over a very small volume of material (see callout on right in Fig. 83.46), the term F_D/A is simply the local shear stress at the part surface. This would give a removal rate description similar to Preston's equation based on the local shear stress (τ) at the part surface

$$\frac{dz}{dt} = C'_p \tau \frac{ds}{dt} \tag{5}$$

Previous work^{22,23} has shown that spot profiles are consistent with the shear stress distribution at the part surface. The remaining two terms in Eq. (5) are not yet fully understood. The relative velocity (ds/dt) is difficult to define in MRF. This velocity could be the relative velocity between the wheel and the part surface, but since the CI in the MR fluid actually supplies the lap, it is more correct that ds/dt is the relative velocity between the CI and the glass surface. This is not easily determined at this time. In fact, the behavior of the different abrasives in different MR fluids may indicate that this relative velocity depends on the abrasive type used. The wheel velocity was the same for all of the experiments described here, so this term was held as constant as possible in terms of controllable experimental parameters.

This work has also shown that, as for other polishing processes, it is difficult to define the Preston coefficient (C'_p) in MRF. This term contains information on the chemistry of the carrier fluid, abrasive type, and glass type. Lambropoulos *et al.*³ showed that the removal rate in MRF is proportional to the term $E/K_c H_K^2$ of the glass (E = elastic modulus, K_c = fracture toughness, and H_K = Knoop hardness of the glass). The experiments described here show that the removal rate depends on the abrasive type as well as the concentration. As a result, this coefficient would also have to contain information about the abrasive type used for a given MR fluid (probably size, shape, and hardness as well as the tribochemical "gripping"¹⁵ power). Finally, it was shown that the presence of DI water dramatically changes how the abrasive interacts with the glass surface. Therefore, information on the chemical make-up of the carrier fluid must also be contained in this coefficient.

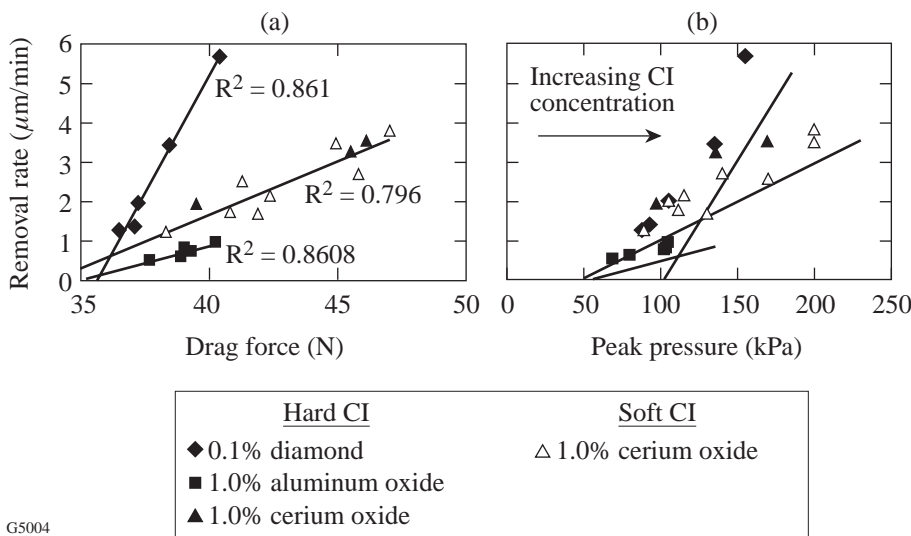
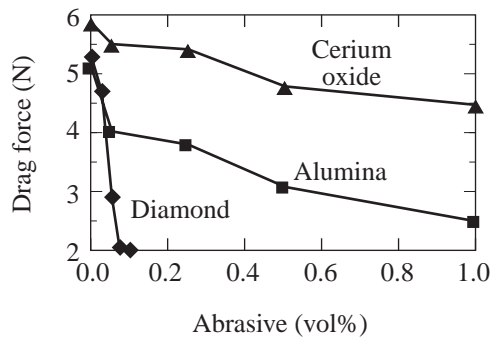


Figure 83.53 Removal rate versus drag force (a), and removal rate versus peak pressure (b). Removal rate increases linearly with pressure and drag force. The linear fits for the drag force go through the origin with high correlation coefficients, but do not for the pressure. This means that there can be removal with a nonzero pressure, but with no drag force (therefore no shear stress) there will be no removal. This supports the idea that shear stress controls removal rate in MRF.

G5004



G5005

Figure 83.54

Effect of adding abrasive to MR fluids 4, 5, and 6 containing 45 vol% CI. In each case the addition of abrasive reduces the drag force, supporting the idea that MRF becomes a three-body abrasion problem. The cerium oxide maintains a high drag force, which supports the theories that cerium oxide has “chemical tooth.”

Summary

The mechanisms of material removal in MRF have been presented. Previous work describes how the shear stress due to the hydrodynamic flow of the MR fluid between the rotating wheel and the part surface controls the removal rate. The idea that material removal depends on the shear stress at the part surface is supported by the linear relation between removal rate and the total drag force shown here. It has also been shown previously that the nanohardness of the CI is important in material removal with nonaqueous MR fluids. We show here that as DI water is added to the MR fluid, the differences in the behavior of the hard and soft CI become less significant as the removal rate dramatically increases for both. This is due to either the presence of a hydrated layer or reduced fracture toughness of the glass in aqueous MR fluids. The addition of nonmagnetic nano-abrasives increases removal rates further since they move to the interface between the CI and the glass surface to control material removal. A transition from two-body to three-body removal is hypothesized. The relative increase in removal depends on the amount and type of the abrasive since different abrasives interact with the glass surface in different ways. This behavior of the abrasive is evident from both AFM scans as well as drag force measurements. More work should allow these results to be summarized in a modified Preston equation based on the local shear stress at the part surface.

ACKNOWLEDGMENT

The authors would like to thank Rebecca Coppens, Henry Romanofsky, Leslie Gregg, Irina Kozhinova, Steven Arrasmith, Caleb Farny, and Susan Brandt of the Center for Optics Manufacturing for their help in this work. We

would also like to thank Alexander Maltsev of LLE for his assistance in sample preparation. Support for this work was provided in part by the Center for Optics Manufacturing (COM), QED Technologies, U.S. Army Materiel Command, and DARPA (Defense Advanced Research Project Agency).

REFERENCES

1. M. J. Cumbo, “Chemo-Mechanical Interactions in Optical Polishing (Glass Finishing),” Ph.D. thesis, University of Rochester, 1993, Chap. 1.
2. M. Buijs and K. Korpel-van Houten, *J. Mater. Sci.* **28**, 3014 (1993).
3. J. C. Lambropoulos, S. D. Jacobs, and J. Ruckman, in *Finishing of Advanced Ceramics and Glasses*, edited by R. Sabia, V. A. Greenhut, and C. G. Pantano, Ceramic Transactions, Vol. 102 (The American Ceramic Society, Westerville, OH, 1999), pp. 113–128.
4. T. S. Izumitani, *Optical Glass*, American Institute of Physics Translation Series (American Institute of Physics, New York, 1986), Chap. 4, pp. 92–98.
5. A. Kaller, *Glastech. Ber.* **64**, 241 (1991).
6. F. W. Preston, *J. Soc. Glass Technol.* **XI**, 214 (1927).
7. W. L. Silvernail and N. J. Goetzinger, *The Glass Industry* **52**, 130 (1971).
8. *ibid.*, 172.
9. T. A. Michalske and B. C. Bunker, *J. Am. Ceram. Soc.* **76**, 2613 (1993).
10. L. M. Cook, *J. Non-Cryst. Solids* **120**, 152 (1990).
11. M. J. Cumbo, D. Fairhurst, S. D. Jacobs, and B. E. Puchebner, *Appl. Opt.* **34**, 3743 (1995).
12. H. Yokota *et al.*, *Surf. Sci.* **16**, 265 (1969).
13. M. Maaza *et al.*, *Opt. Commun.* **100**, 220 (1993).
14. A. B. Shorey, K. Xin, K.-H. Chen, and J. C. Lambropoulos, in *Inorganic Optical Materials*, edited by A. J. Marker III (SPIE, Bellingham, WA, 1998), Vol. 3424, pp. 72–81.
15. A. Kaller, *Glass Sci. Technol.* **71**, 174 (1998).
16. N. B. Kirk and J. V. Wood, *J. Mater. Sci.* **30**, 2171 (1995).
17. D. Golini, S. Jacobs, W. Kordonski, and P. Dumas, in *Advanced Materials for Optics and Precision Structures*, edited by M. A. Ealey, R. A. Paquin, and T. B. Parsonage, Critical Reviews of Optical Science and Technology (SPIE, Bellingham, WA, 1997), Vol. CR67, pp. 251–274.
18. S. D. Jacobs, S. R. Arrasmith, I. A. Kozhinova, L. L. Gregg, A. B. Shorey, H. J. Romanofsky, D. Golini, W. I. Kordonski, P. Dumas, and S. Hogan, in *Finishing of Advanced Ceramics and Glasses*, edited by R. Sabia, V. A. Greenhut, and C. G. Pantano, Ceramic Transactions, Vol. 102 (The American Ceramic Society, Westerville, OH, 1999), pp. 185–199.

19. S. R. Arrasmith, I. A. Kozhina, L. L. Gregg, A. B. Shorey, H. J. Romanofsky, S. D. Jacobs, D. Golini, W. I. Kordonski, S. J. Hogan, and P. Dumas, in *Optical Manufacturing and Testing III*, edited by H. P. Stahl (SPIE, Bellingham, WA, 1999), Vol. 3782, pp. 92–100.
20. S. D. Jacobs, W. Kordonski, I. V. Prokhorov, D. Golini, G. R. Gorodkin, and T. D. Strafford, “Magnetorheological Fluid Composition,” U.S. Patent No. 5,804,095 (8 September 1998).
21. Zygo Mark IVxp™ or Zygo GPI xpHR™ phase-shifting interferometer system was used for all data acquisition and analysis related to polishing spots, HeNe laser source with $\lambda = 632.8$ nm, Zygo Corporation, Middlefield, CT 06455.
22. V. W. Kordonski, D. Golini, P. Dumas, S. J. Hogan, and S. D. Jacobs, in *Smart Structures and Materials 1998: Industrial and Commercial Applications of Smart Structures Technologies*, edited by J. M. Sater (SPIE, Bellingham, WA, 1998), Vol. 3326, pp. 527–535.
23. A. B. Shorey, “Mechanisms of Material Removal in Magnetorheological Finishing (MRF) of Glass,” Ph.D. thesis, University of Rochester, 2000, Chap. 3.
24. *ibid.*, Chap. 2.
25. A. B. Shorey, W. I. Kordonski, S. R. Gorodkin, S. D. Jacobs, R. F. Gans, K. M. Kwong, and C. H. Farney, *Rev. Sci. Instrum.* **70**, 4200 (1999).
26. Q22, QED Technologies, LLC, Rochester, NY 14607.
27. Field measurements were taken with the F. W. Bell Model 9500 Gaussmeter, Bell Technologies Inc., Ontario, FL 32807.
28. Computrac Max-1000 moisture analyzer, Arizona Instruments, Phoenix, AZ 85040-1941.
29. Brookfield DV-III cone and plate viscometer, Brookfield Engineering Laboratories, Inc., Stoughton, MA 02072.
30. Zygo NewView™ White Light Optical Profiler, areal over 0.25 mm \times 0.35 mm with a 20 \times Mirau objective, 1.1- μ m lateral resolution, Zygo Corporation, Middlefield CT 06455.
31. Nanoprobe III atomic force microscope (AFM), Digital Instruments, Santa Barbara, CA 93117.
32. Measured with the I-scan pressure measurement system, Tekscan, Inc., Boston, MA 02127. We used a 0.1-mm-thick 5051 pressure film with a maximum allowable load of 345 kPa (50 psi) and a lateral resolution of 1.27 mm.
33. Linear ball slide, Parker Hannafin Corporation, Cleveland, OH 44124-4141.
34. LKCP475 5-lb load cell, Cooper Instruments, Warrenton, VA 20188.
35. A. B. Shorey, K. M. Kwong, K. M. Johnson, and S. D. Jacobs, *Appl. Opt.* **39**, 5194 (2000).
36. A. B. Shorey, L. L. Gregg, H. J. Romanofsky, S. R. Arrasmith, I. Kozhina, J. Hubregesen, and S. D. Jacobs, in *Optical Manufacturing and Testing III*, edited by H. Stahl (SPIE, Bellingham, WA, 1999), Vol. 3782, pp. 101–111.
37. Corning 7940, Corning, Inc., Corning, NY 14831-0002.
38. R. S. Higgins and S. A. Kilinger, *High Purity Solvent Guide*, 3rd ed. (Baxter Diagnostics, Muskegon, MI, 1990).
39. Brookfield DV-II Digital Viscometer, Brookfield Engineering Laboratories, Inc., Stoughton, MA 02072.
40. A. B. Shorey, “Mechanisms of Material Removal in Magnetorheological Finishing (MRF) of Glass,” Ph.D. thesis, University of Rochester, 2000, Chap. 5.
41. NanoTek Cerium Oxide, Nanophase Technologies Corporation, Burr Ridge, IL 60521.
42. NanoTek Aluminum Oxide, Nanophase Technologies Corporation, Burr Ridge, IL 60521.
43. 0.125- μ m Hyprez-type PC diamonds, Engis Corporation, Wheeling, IL 60090.
44. NanoTek Cerium Oxide and Aluminum Oxide product literature of Nanophase Technologies Corporation, Burr Ridge, IL 60521, <http://www.nanophase.com/products.shtml>.
45. I. Kozhina, L. Gregg, and J. Hesterman, “CPD-012 Cerium Oxide Powder Particle Size Measurements Using the Variety of Relative Refractive Indexes,” Magnetorheological Finishing Laboratory internal report, Center for Optics Manufacturing, Rochester, NY, 25 February 2000.
46. “Fundamentals of Particle Sizing,” product literature of Nanophase Technologies Corporation, Burr Ridge, IL 60521.
47. Engis diamond product literature, Engis Corporation, Wheeling, IL 60090, <http://www.engis.com/hyprez/powders.html>.